Suplemento de la Revista Mexicana de Física **4** 021133 (2023) 1–7

Implementation and improvement of image reconstruction techniques using muons from cosmic rays

J. Villalobos Alva[a], C. Uribe Estrada[b], C. Arturo Angeles[a] and M. Ramírez García[a]

[a] *Universidad Iberoamericana Ciudad de México, Lomas de Santa Fé, México, 01219.*

[b] *Instituto de Ciencias, Benemérita Universidad Autónoma de Puebla, Ciudad Universitaria. Puebla, Pue., México 72570.*

Received 14 May 2023; accepted 29 November 2023

In this article, two image reconstruction techniques for radiography and tomography using cosmic ray muons are presented. The simulation is carried out using the `Geant4` package, simulating a multiple coincidence system of four RPCs (Resistive Plate Chambers). The reconstruction techniques presented are based on particle trajectory reconstruction and localization of a single center of dispersion. Two functional cases are displayed for each technique.

Keywords: Imaging techniques; muon radiography; muon tomography; tracking detectors; Monte Carlo simulation.

DOI: https://doi.org/10.31349/SuplRevMexFis.4.021133

1. Introduction

Cosmic rays are highly energetic atomic nuclei or other particles traveling through space at relativistic speed. These very high energy particles interact with the earth's atmosphere generating showers of elementary particles (cosmic ray showers); within the particles produced, the muon ($\mu^{\pm}$) is a particle of great interest [1]. These atmospheric muons have been employed as imaging tools, such as muon radiography and muon tomography [2]. Methods such as the latter have supplied an effective way to gain an understanding of the inner layout of objects with non-invasive technologies [3]. Here we present the outcome of the reconstruction algorithm, implemented for image reconstruction, by collecting the position information of the registered hits on an impacted 4-RPC (Resistive Plate Chamber) detection system and signal filtration. The reconstruction techniques presented are based on particle trajectory and localization of the single center of dispersion (POCA) [4], with the extension threshold procedure for better image resolution. Using Monte Carlo simulation in the `Geant4` toolkit [5] two case examinations for muon radiography and muon tomography are presented.

2. Geometry framework configuration

2.1. RPC Detector layout

As a primary tracking detector, the single gap Bakelite plate (high resistivity $10^{10} - 10^{12}$ Ωcm [6]) RPC was designed, with a large functional coverage area.

The surface of the RPC has an operative area of 1×1 m^2. Each RPC plate was simulated with an Ar:CO_2 gas mixture, with ratios of 70:30 respectively. The gas mixture gap is 2 mm, resembling the same space as the one proposed by Santonico and Cardarelli [7].

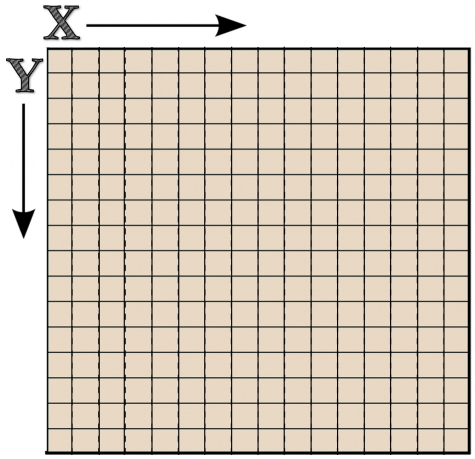

FIGURE 1. Matrix division representation of the RPC detector.

Each RPC panel is based on strip division, which constructs a matrix as shown in Fig. 1. Each matrix detector comprises the construction of an orthogonal series in the X and Y directions producing subdivisions in 25 equal parts. This creates a primitive grid cell of 4×4 cm^2 derived from the division of the series of each axis, providing a sensing facet with the capability of measuring the number of particles. This allows the reconstruction of each track of the particles that cross all detectors. A general 4-fold coincidence detection system was created for the radiography and tomography simulations. This was used for selecting signals which match the detection of a muon in each of the four detectors, ensuring correct measurements and false hit discriminate position for each muon ray.

2.2. Radiography outline

For the radiography case scenario, each RPC detector was placed with an inter-panel difference of 8 cm, retaining a dis-

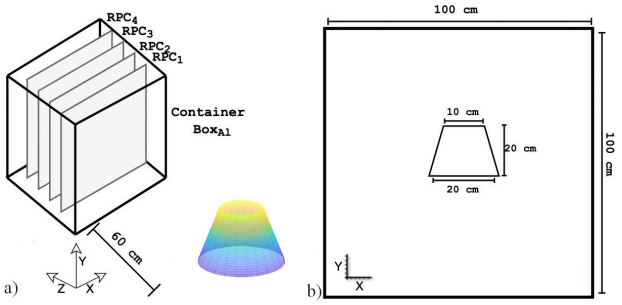

FIGURE 2. a) Isometric schematics of the stack model. b) XY projection of the whole stack model detection system.

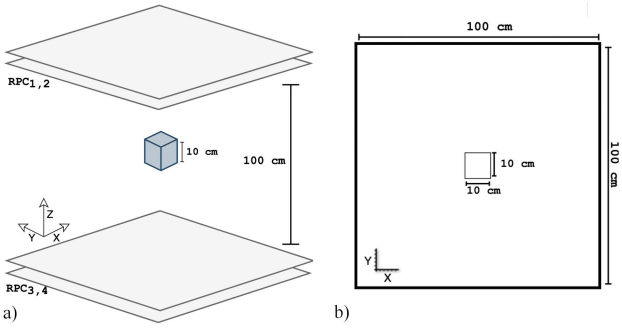

FIGURE 3. a) Isometric diagram of the target (Pb cube) located in the center between RPC plates, evenly spaced. b) A view of the XY plane that shows the size of the RPC trackers and the target.

tance of 24 cm between the front and rear panels, as exhibited in Fig. 2. Each detection surface is capable of measuring the number of events, allowing the reconstruction of each track of the particles that cross each grid surface.

2.3. Tomography outline

The design schematics of the tomography case are shown in Fig. 3, consisting of 4-RPC tracking detectors, with two pairs of detectors divided to assemble an upper detection zone (entrance) and a bottom detection zone (exit). This creates a region of interest, composing an enclosed sector bounded by the 2 inner detectors for every detector recording the hit position in each orthogonal series (X,Y), similar to the RPC radiography.

3. Geant4 simulation

3.1. Muon data generation

The Monte Carlo simulation was tested using the Geant4 programming toolkit. The implementation consists of the following steps to construct the two case scenarios (radiographic and tomographic imaging). Cosmic ray muon runs were conducted for 2 different setups. Figure 4 illustrates each scenario simulated in Geant4, taking into consideration the following factors:

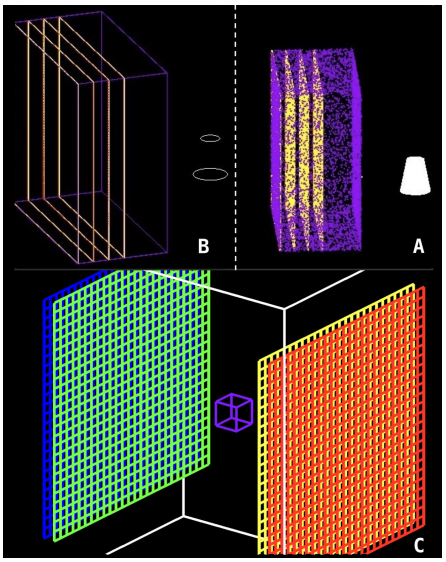

FIGURE 4. Geant4 simulation view of the detector station system and targets. All figures present the objects to examine. Figures A and B exhibit the radiographic layout. Figure C shows the tomographic configuration.

- The first simulation (with $\sim 50,000$ events) was performed with a volume between the source and the 4-RPC system for a concrete trapezoid ($\rho = 2.3$ g/cm^3) with dimensions of $h = 40$ cm, $b_{inf} = 20$ cm, and $b_{\text{sup}} = 10$ cm.
- The second run was performed for $\sim 40,000$ events using a $10 \times 10 \times 10$ cm^3 lead block (Pb, Z=82).

Muons were generated with the proper energy and angular distributions from cosmic rays. For the scenarios handled, the EcoMug.h [8] header library was used, allowing the creation of cosmic ray muon flux and providing the ability to generate angular distributions from different surfaces (from which the muon is created) established by the user. Here, the plane-based generation method was as a plane-flat sky, maintaining the correct angular distribution of $\cos^2$ and the correct moment, with the intent that the majority of occurrences were able to propagate through the whole 4-fold tracking detectors, recording the positional information as particles traverse each detector. The generation starts with the initialization of each event generated by the primary particles, specifying the minimum and maximum values for the zenith angle, $\theta \in [0, \pi/4]$, and azimuthal angle $\phi \in [0, \pi]$.

3.2. Data flow acquisition

The Ecomug configuration is contained in the Primary Genereation Action class, which tells the Geant4 kernel how to perform the distribution and flow of muon data. The data acquisition is obtained from the records of the entire detection system. The *Geant4* Histomanager driver is used as the data control component which creates, reads and formats the Monte Carlo simulation files, saving the information in a root format file.

4. Detection and image reconstruction

Utilizing the results from each simulation, the imaging object reconstruction was carried out for both models by implementing python programming scripts.

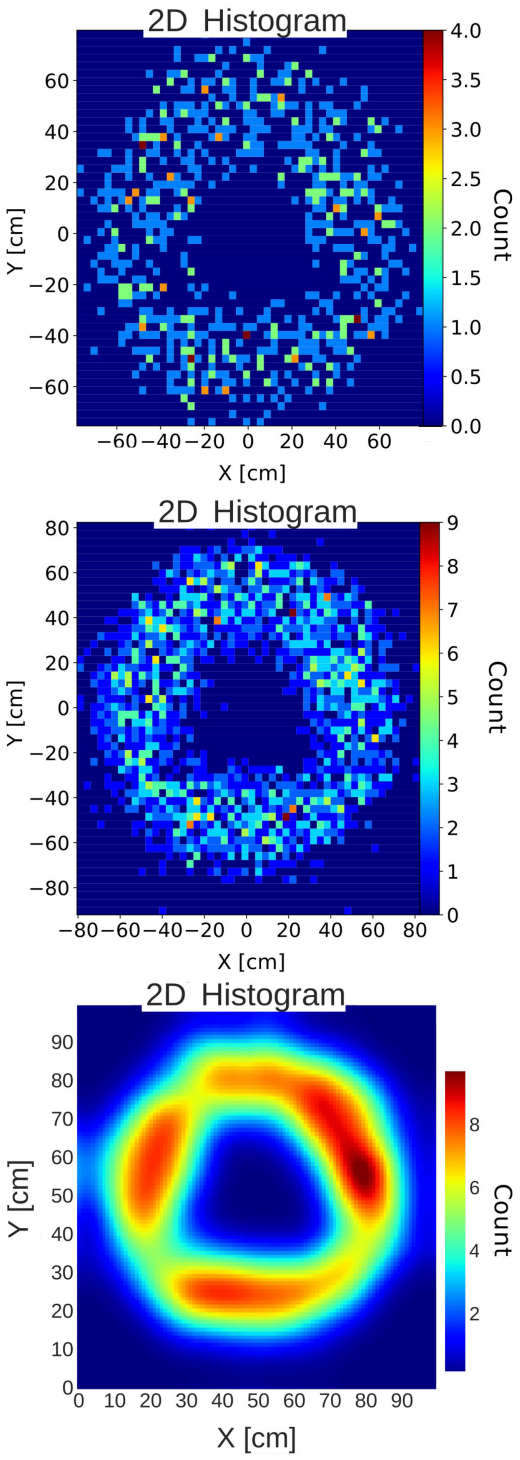

FIGURE 5. Figures a) to c) show a 2D reconstruction of the target for muon radiography. The muon count increases in every image, starting from a) to c).

4.1. Radiography reconstruction

All event data was processed from the individual records of the detectors. Hit data patterns in the X and Y series in the layers were recorded through which the sensitive detector was triggered. Filters were implemented with the condition that the layer-wise timing increases ($t_n \leq t_{n+1}$) as the ray hits the first detector ($n = 1$) to the last one ($n = 4$). Once filtered, the selected hits per layer are regarded as the muon signal path. The data is then set to be fitted separately in the planes ZX and ZY as straight lines:

$$f(z)_{x,y} = m_{x,y} \cdot z + b_{x,y}, \quad \text{for } i = 0 \ldots N_{\mu}, \quad (1)$$

where m is the slope, b is the intercept, and x, y and z are the corresponding coordinates.

Figure 5 can be depicted as a solid material. The image results allowed us to accurately reconstruct the image, revealing a clear profile of the surface of the object.

The graphics presented provide clear evidence of a deflection zone. Within this zone, enclosed only by the presence of air, certain impacts are unequivocally observed. We firmly believe that these anomalies are a direct result of misleading signals. The muon flux, on occasion, fails to reach all four RPC detectors, giving rise to these outliers. However, it is crucial to note that the presence of this zone does not signify the absence of a simulated object. The signals detected within the expected boundaries of the entity may indeed be muons that experienced slight scattering near the edges of the object. Hence, it is apparent that the iterative fitting process itself may also contribute to the generation of these misleading signals through the coordination of track pairs for each iteration of reconstructed points around those areas.

4.2. Tomography reconstruction

For the tomography case, the image reconstruction method was conducted using the point of closest approach algorithm [4], consisting of finding the closest point from the linear muon tracks (entrance/exit track). The track sampling is attained by the series of hits as the ray reaches the top and bottom layout ($n = 1 \ldots 4$), as time increases during flight ($t_n \leq t_{n+1}$). Respective upward and downward tracks are computed by the least squares fitting technique of the coordinates of impact (x, y, z) of the tracks on the detector plane, with the z coordinate representing the depth position of the respective RPC plates. The two fitted tracks of the muon are used to calculate the total angle of dispersion by finding the shortest distance between them and computing its midpoint (dispersion point), which is known as the POCA coordinate point. The algorithm excludes the events that do not traverse the 4-fold detection system and which have a dispersion angle smaller than 10 mrad (noise events). Figure 6 shows the 3D reconstruction pattern, where each point represents the single point of dispersion of the muon ray, deflected by the presence of the target in the probe region. The majority of

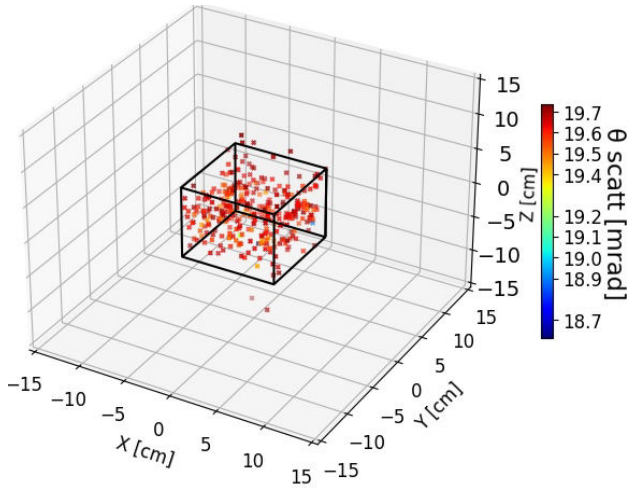

FIGURE 6. 3D hit imprint reconstruction POCA points, above $\theta_{\text{threshold}} \geq 10$ mrad representing the angle deflection given the scenario target. The hue pattern encodes the magnitude of the deflection angle, where greater magnitudes are colored by red tones and lesser by blue tones. The black colored edges of the cube designate the limits of the position of the simulated Pb cube.

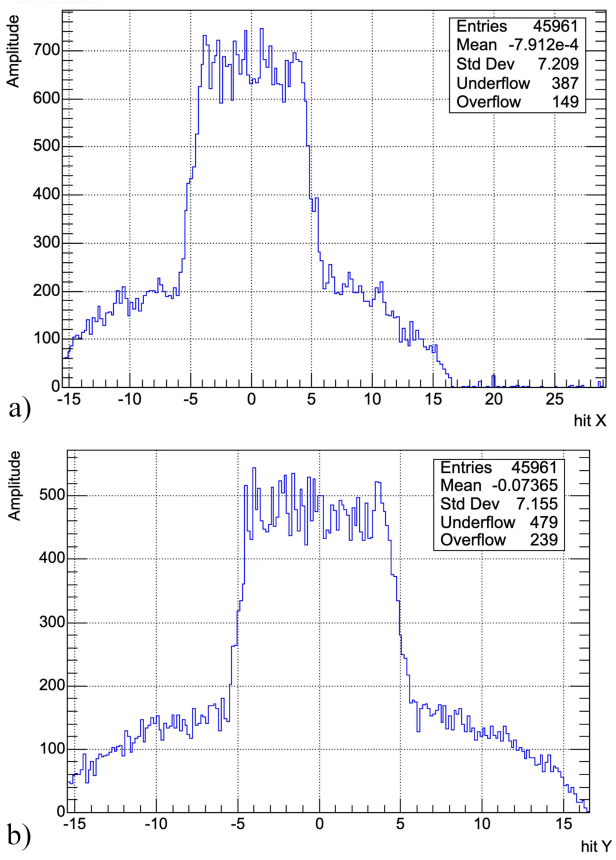

FIGURE 7. Muon hit pattern for X and Y coordinates of the 4RPC detection system.

POCA points are correspondingly reconstructed, primarily at the localization of the target inside the region of interest.

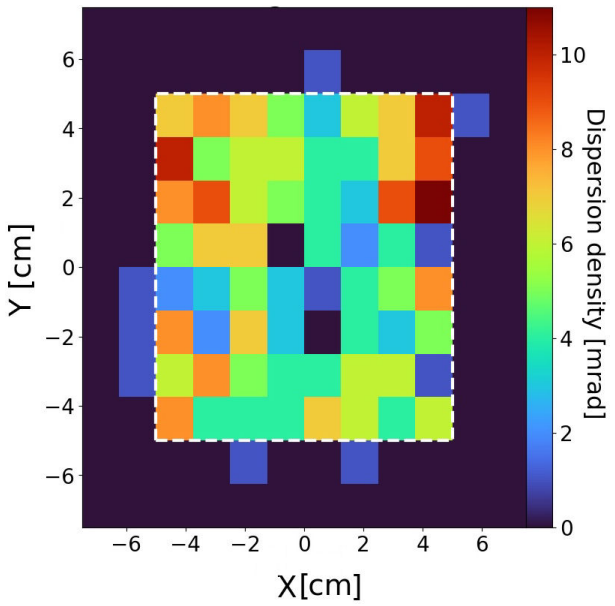

FIGURE 8. 2D view of the reconstructed probe. Additional muon scattering outside the main target might be caused by the external material, producing inaccurate POCA with low dispersion angles.

The representation of the simulated location cube can be seen in Fig. 6. The probe stands out from the surroundings and the majority of the POCA dispersion points are fairly reasonably imaged within the limits of the simulated cube edges. It is not expected to observe scattering points beyond the object (the cube). Nonetheless, in some instances, these points might emerge as false paths of muons and deceptive dispersion resulting from interactions with air as seen in the graphic.

In this case, the object stands out, as being the sole target in the region of interest and the target localization is resolved as the complementary x and y line profile distributions shown in Fig. 7.

The 2D top view projection of the xy plane ($z = 0$) portrays the mean dispersion density angle (mrad). In particular, the contour lines indicate the outline border of the cube. As seen in a great number of muons are found within the enclosed region of the cube.

5. Conclusion and future work

From the simulated scenarios, tangible target imaging was achievable by the presented algorithm and simulations. Enough ray statistics were gathered, allowing the discrimination of the surface profiles of the geometric object with enough sharpness to resolve smoother profiles. Additionally, these validate the location of the volumetric object along with the complementary graphs of the profile distributions. Accordingly, by the reduction of false signals in combination with the 4-fold detector and angle threshold boundary, both results create reasonable study cases. As for the future, conducting different scenarios with distinct materials, prototypes

can be implemented and algorithm improvement can be accomplished by lowering the angle dispersion threshold and accumulating greater scattering data by adding more values along the z-axis.

Acknowledgements

Work supported by project No. A1-S-39980, CB-2017-2018 CONACyT, Mexico.

1. G. Bonomi *et al.*, Applications of cosmic-ray muons, *Prog. Part. Nucl. Phys.* **112** (2020) 103768, https://doi.org/10.1016/j.ppnp.2020.103768.
2. L. Bonechi, R. D'Alessandro, and A. Giammanco, Atmospheric muons as an imaging tool, *Rev. Phys.* **5** (2020) 100038, https://doi.org/10.1016/j.revip.2020.100038.
3. S. Procureur, MMuon imaging: Principles, technologies and applications, *Nucl. Instrum. Methods A* **878** (2018) 169, https://doi.org/10.1016/j.nima.2017.08.004.
4. W. Zeng *et al.*, Principle study of image reconstruction algorithms in muon tomography, *JINST* **15** (2020) T02005, https://doi.org/10.1088/1748-0221/15/02/T02005.
5. S. Agostinelli *et al.*, Geant4-a simulation toolkit, *Nucl. Instrum. Methods A* **506** (2003) 250, https://doi.org/10.1016/S0168-9002(03)01368-8.
6. A. Sharma, Muon tracking and triggering with gaseous detectors and some applications, *Nucl. Instrum. Methods A* **666** (2012) 98, https://doi.org/10.1016/j.nima.2011.12.001.
7. R. Santonico and R. Cardarelli, Development of resistive plate counters, *Nucl. Instrum. Methods A* **187** (1981) 377, https://doi.org/10.1016/0029-554X(81)90363-3.
8. D. Pagano *et al.*, EcoMug: An Efficient COsmic MUon Generator for cosmic-ray muon applications, *Nucl. Instrum. Methods A* **1014** (2021) 165732, https://doi.org/10.1016/j.nima.2021.165732.